Placenta 182 (2026) 330–340

Contents lists available at ScienceDirect

Placenta

journal homepage: www.elsevier.com/locate/placenta

Multi-scale computational models of intervillous blood flow in fetal growth restriction: implications of anatomical changes on syncytiotrophoblast shear stress

Tet Chuan Lee [a], Teena K.J.B. Gamage [b], Mary Spring [b], Isha Ramanlal [b], Toby Jackson [c], Alys R. Clark [c], Joanna L. James [b,*]

[a] Department of Mechanical Engineering, Auckland University of Technology, 31 Symonds St, Auckland, New Zealand
[b] Department of Obstetrics, Gynaecology and Reproductive Sciences, Faculty of Medical and Health Sciences, University of Auckland, 85 Park Rd, Grafton, Auckland, New Zealand
[c] Auckland Bioengineering Institute, University of Auckland, 70 Symonds St, Auckland, New Zealand

ARTICLE INFO

Keywords:
Intervillous space
Syncytiotrophoblast
Shear stress
Mechanosensing
Fetal growth restriction

ABSTRACT

Introduction: The haemodynamics of maternal blood flow in the intervillous space (IVS) impacts placental exchange efficiency. The resulting shear stress can also affect syncytiotrophoblast function, and in turn placental development. Here, we use anatomically-informed multiscale modelling approaches to predict flow in the IVS and syncytiotrophoblast shear stress in fetal growth restriction (FGR).

Methods: Three-dimensional placentone models were established and parameterised to normal and FGR scenarios. Normal term and FGR placental tissue punches were microCT imaged, segmented, and used in tissue-level computational fluid dynamics simulations to predict syncytiotrophoblast shear stress. Tissue and placentone-level models were combined to predict syncytiotrophoblast shear stress ranges. Mechanosensing protein expression was determined by immunohistochemistry.

Results: Placentone-level models demonstrate variation in IVS flow velocity across the placental depth, with higher velocity regions at spiral artery mouths that extended further in FGR. Tissue-level models predicted higher levels of syncytiotrophoblast shear stress in FGR. Combined models predicted a greater proportion of tissue is exposed to higher shear stresses in FGR, with ~2-fold increase in peak shear stress proximal to spiral artery openings. Including septal veins increased penetration of maternal blood and the proportion of tissue exposed to higher shear. In FGR, the syncytiotrophoblast had greater Dynein-1 and lower Kinesin-2 and TRVP6 expression, but no difference in IFT88, Polycystin-2 or Piezo-1 expression.

Conclusions: In FGR, impaired remodelling of the spiral arteries and changes in villous tissue architecture combine to increase the proportion of placental tissue exposed to higher shear stress. Septal veins and central cavities act synergistically to ensure adequate placental perfusion.

1. Introduction

Fetal growth restriction (FGR, babies <3rd growth centile) is a significant clinical issue with no effective treatment other than preterm delivery [1]. Over 50% of FGR cases are not detected prior to delivery, making FGR the largest risk factor for stillbirth [2]. The pathophysiology of FGR is established in early pregnancy, but is clinically silent until at least mid-gestation, making this disorder particularly challenging to predict or treat.

The placenta has a branched villous structure. Fetal blood circulates in vessels within the villous branches, and for most of pregnancy maternal blood from the uterine spiral arteries perfuses around the outside of the villi in the intervillous space (IVS). Exchange between these physically separate circulations occurs across the trophoblast bilayer (comprising the inner cytotrophoblast and outer syncytiotrophoblast) that encases the placental villi. FGR occurs due to poor placental exchange due to a heterogenous combination of factors, including reduced placental branching, impaired development of the feto-placental vasculature, reduced remodelling of the uterine circulation, changes in speed and volume of IVS blood flow, a thicker

* Corresponding author.
E-mail address: j.james@auckland.ac.nz (J.L. James).

https://doi.org/10.1016/j.placenta.2026.07.007
Received 15 February 2026; Received in revised form 29 June 2026; Accepted 13 July 2026
Available online 13 July 2026

syncytiotrophoblast with altered cell turnover, and reduced syncytiotrophoblast nutrient transporter expression [3]. That many of these factors converge on the IVS highlights its potential importance in the pathogenesis of FGR.

The nature of IVS blood flow is governed by two factors: the architecture of the placental villous tree around which the blood flows, and the velocity and volume of blood entering the IVS from the uterine circulation. We, and others, have developed computational predictions of flow in the IVS in normal pregnancies at term, enabling prediction of the range of shear stress (the force arising from blood flow that acts parallel to the cell surface) on the syncytiotrophoblast across the IVS [4–6]. Our previous work also extended such models to earlier gestational scenarios, demonstrating that the range of shear stress experienced by the syncytiotrophoblast in the late first-trimester is in fact slightly higher than that at term, and highlighting the important impact of villous architecture on flow in the IVS [6]. FGR placentae are characterised by impaired villous development, reducing the density of villi, and changing the architecture of the IVS [3,7,8]. However, whilst computational models have highlighted the impact of altered spiral artery remodelling in FGR on IVS flow in a single placental geometry [5], the impact of varying placental architecture in FGR has not been explored.

In addition to villous architecture impacting shear stress, shear stress itself may impact placental development and function. Indeed, shear stress and mechano-signalling play important roles in vascular remodelling/function and tissue morphogenesis during development in other organs [9,10], and in placental models has been linked to increased rates of syncytialisation [11] and shifts in metabolic pathways [12]. The syncytiotrophoblast expresses a range of mechanosensing proteins across gestation, with increased expression in late first trimester placentae compared to term [6,13,14]. Such proteins have been demonstrated to functionally impact the syncytiotrophoblast, for example TRPV6 knockdown impacts intracellular calcium signalling and alteration of microvillus formation [13]. Together, this demonstrates that the placenta can dynamically respond to IVS haemodynamics from early in gestation, and provides a further potential mechanistic link between altered IVS haemodynamics in FGR and impaired placental function. However, the expression of mechanosensing proteins in pregnancy pathologies has not been investigated, and the relative role of alterations in syncytiotrophoblast shear stress, and alterations in the ability of the syncytiotrophoblast to respond to this shear stress are unknown.

Here, we employ three-dimensional (3D) micro computed tomography (microCT) imaging of placental villi to parameterise our *in silico* models of flow in the IVS to pathological FGR scenarios at the villous and placentone scales, enabling us to predict the range of shear stress on the syncytiotrophoblast in FGR. We also demonstrate alterations in mechanosensing protein expression by the syncytiotrophoblast of FGR placentae for the first time, suggesting that the ability of the syncytiotrophoblast to respond to shear stress may be altered in FGR, and highlighting the importance of dynamically interacting uterine and placental components in this disorder.

2. Methods

2.1. Placental collection

The use of all placentae in this work was approved by the HDEC Northern X Ethics Committee (NTS/12/06/057/AM09). Placentae were obtained following written informed consent from Auckland City Hospital. FGR pregnancies were recruited into the study if their estimated fetal weight was <10th growth percentile, and placentae from these pregnancies were included in the study if their birthweight was <3rd customised growth percentile (the norm in the New Zealand healthcare system, which adjusts birthweight for maternal ethnicity, parity, height and weight as per [15]). Normal placentae used in this study were matched for gestational age and >20th customised birthweight percentile. Exclusion criteria for all third-trimester placentae (normal and FGR) were; multiple pregnancies, pre-eclampsia, hypertension, diabetes, autoimmune disease, recent COVID infection, and/or maternal BMI >30 kg/m^2.

2.2. Structural analysis of placental tissue - tissue preparation and microCT imaging

FGR (n = 5) and gestational age-matched normal third-trimester placentae (n = 5) were used for microCT analysis (clinical details provided in Supplementary Table 1). A full depth 8 mm diameter tissue punch was taken from the maternal aspect of the centre of each placenta, fixed in 4% paraformaldehyde, washed in 70% ethanol, and stained for 9 days with 0.3% phosphotungstic acid in 70% ethanol, as previously described [6]. Prior to imaging tissue was washed in 70% ethanol for 24 h, dehydrated in an ethanol series (80%, 90% 100% ethanol), then stored in 100% ethanol at room temperature for 24 h to remove excess water within the sample that absorbs X-rays, and can cause imaging artifacts.

Tissue punches were positioned between two rounds of ethanol dampened polystyrene within an 8 mm diameter plastic straw, with tissue paper saturated in 100% ethanol placed on top of each sample to prevent it drying out. Each sample was wrapped in 4 layers of Mylar tape, and imaged in a Bruker Skyscan 1272 microCT, with a custom aluminium filter used. The voltage (kV) and current (μA) for microCT ranged from 75 kV:128 μA to 85 kV:113 μA depending on the size and density of the sample. Exposure time was also sample dependant, ranging between 1500 and 2000 ms. The samples were imaged over 360° rotation with a 0.275° rotation step. Averaging was done over two frames and random movement was set at 4 pixels. The samples were imaged with an isotropic voxel size of 5.5 μm with the scan time approximately 3 h per field of view. Due to the height of the sample, oversize scanning was conducted with multi-part scanning over 2-3 fields of view. Images were reconstructed using NRecon software (version 1.7.4.2, Bruker, Belgium).

2.3. Structural analysis of placental tissue - image processing

Tissue architecture was analysed in equally sized 273x273x273 pixel (1.5x1.5 × 1.5 mm) cubes selected at random from the list of cubes that do not sit at the edge of the sample, to avoid any bias from artifacts at tissue edges due to acquisition of tissue punches. These cubes were generated via creation of a mosaic map of the central trans-axial image projection. Villous tissue was semi-automatically segmented using ITK-Snap [16]. First, the active contour segmentation tool, initialised via a manually selected threshold, was used to compute an initial segmentation. As tissue staining predominantly targets the villous surface, manual corrections were required to fill unfilled villous cores due to lack of staining in larger villi, and to separate villi in very close proximity that were joined together during automatic segmentation. Manual corrections were done slice by slice in the X-Y plane, leading to thin erroneous connections and inconsistencies along the X-Z and Y-Z planes. To address this, binary opening was done with a 5-voxel line kernel, in line in the Z axis. Further smoothing was done using binary opening, utilising a binary ball kernel, with a diameter of three voxels.

To inform model assumptions that tissue architecture does not vary across different depths of tissue, analysis of differences in villous architecture were first undertaken from the near-maternal, central, and near-chorionic aspects of microCT imaging datasets of tissue punches from 4 normal and 5 FGR placentae. No significant differences in volume fraction or surface area to volume ratio were evident between the three different regions (Supplementary Fig. 1).

2.4. Computational models

Computational models were employed to relate villous architecture to villous surface shear stress, as described in detail by Lee et al. [6]. The modelling framework incorporates a porous *medium model* and a *villous tissue model*, which are then combined to predict distributions of shear stress at the placentone scale. The porous medium model represents the placentone (a functional unit of the placenta) fed by a spiral artery and drained by decidual veins. This model allows prediction of regional maternal blood pressure drops across villous tissue units of the scale analysed from microCT. The villous tissue model then provides direct characterisation, for a fixed maternal blood pressure drop of the distribution of shear stress in an imaged tissue cube. Finally, the two models are combined to predict the overall distribution of villous surface (syncytiotrophoblast) shear stress in a placentone.

Porous medium model: The placentone has previously been modelled in 2D [4,6,17] and 3D [5,18–20]. Here we adopt a 3D model with a square cross-section [18], illustrated in Fig. 1A, with a height Z_p and width in both directions of X_p, and considered to represent a centrally located placentone rather than one on the periphery of the placenta. The spiral artery feeding the placentone is modelled as a funnel shaped opening whose diameter increases from d_A to d_M over a length L_B. Two decidual veins are located at a distance $x_p/4$ on either side of the spiral artery and have a diameter of d_V. The internal volume of the placentone is considered a porous medium with porosity ϕ, except in an elliptical region immediately distal to the spiral artery of height L_{cc} and width d_C+2d_{extra} representing a central cavity. The porous medium model was implemented in Ansys Fluent (Ansys Inc., 2022 R2) with the viscous model set to laminar and the porous domain set as a porous zone with fluid porosity and viscous resistance (taken to be the inverse of the permeability) set as in Table 1. The porous medium model predicts blood flow velocity (Fig. 1B and C) and local pressure gradients (Fig. 1D and E).

The porous medium model was implemented in the following scenarios:

1. Using geometric parameters for a normal term placenta (Table 1). Blood flow velocity at the spiral artery mouth was fixed, following prior studies [6].
2. Using geometric parameters modified to represent an FGR placenta (Table 1) where the spiral artery dimensions are reduced by half to represent an inadequately remodelled spiral artery. Inlet volume flowrate was prescribed, and taken to be either the same as the normal placenta (computed from scenario 1) or reduced to 75% of this value.

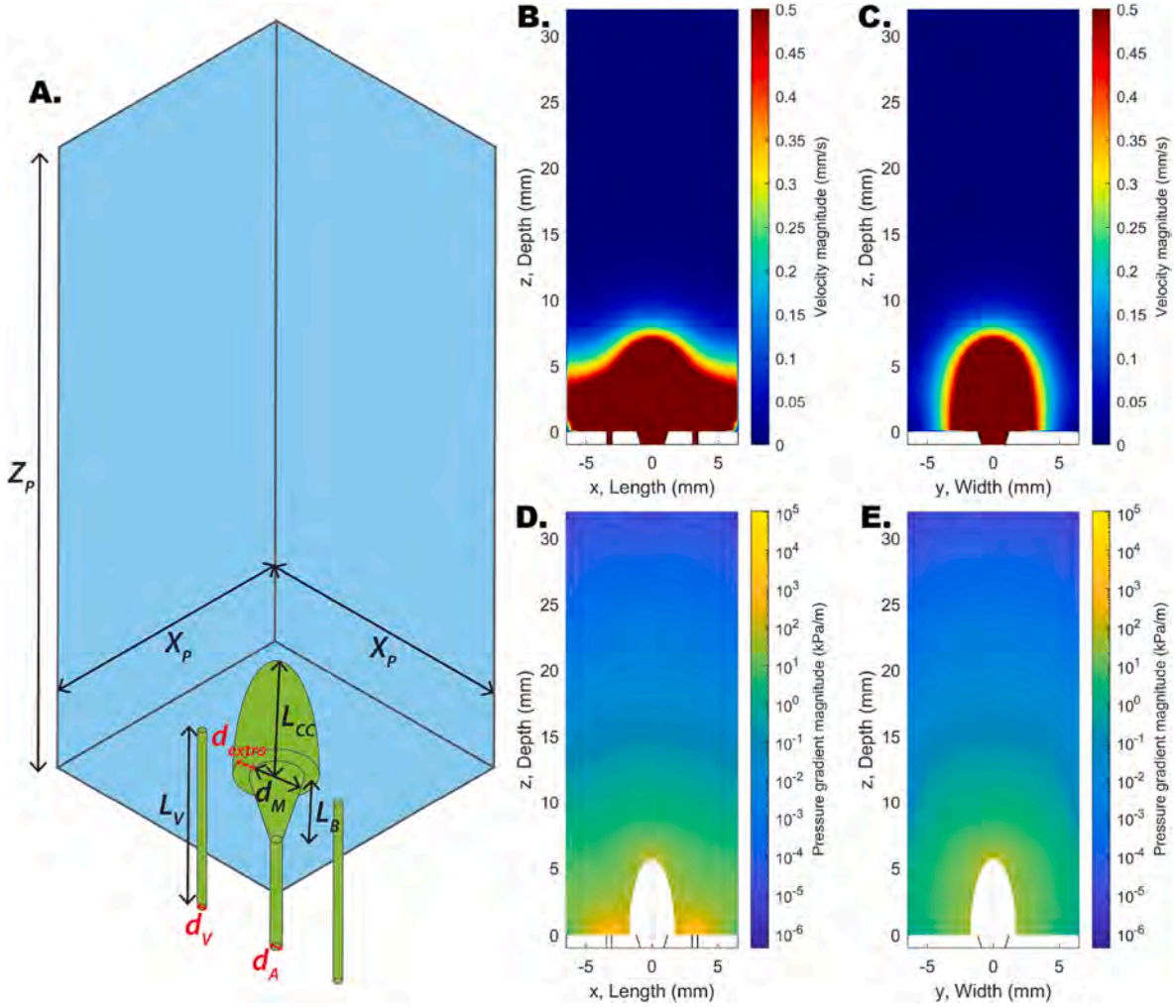

Fig. 1. A) Geometry of 3D porous medium model of the placentone, which consists of an inlet remodelled spiral artery, a central cavity and two decidual veins that serve as outlets, which feed and drain a porous placentone. The velocity (B, C) and pressure gradient (D, E) obtained from simulations of the placentone model under normal (baseline) parameters, which are similar to those produced by Lee et al. [6] but extrapolated to 3D. (B, D) shows results for a plane that passes through the centre of the placentone going through the decidual veins while (C, E) shows the results for a plane that passes through the centre of the placentone perpendicular to this.

Table 1
Parameters used to create the porous media model.

Parameter	Normal	FGR	References
Blood density, ρ	1056 kg/m^3		[21]
Blood viscosity, μ	0.003 Pa.s		[21]
Spiral artery diameter, d_A	0.5 mm	0.25 mm	[22]
Spiral artery mouth diameter, d_M	2.4 mm	1.2 mm	[23,24]
Decidual vein diameter, d_V	0.4 mm		[18]
Central cavity extra width, d_{extra}	0.5 mm		[18]
Spiral artery remodelling length, L_B	3 mm		[24]
Central cavity height, L_{CC}	5.63 mm		[18]
Placentone height, Z_L	32 mm		[25,26]
Placentone width, X_L	13 mm		[18]
Mean Velocity at spiral artery mouth	0.14 m/s	Taken to have the same inlet flow rate into the spiral artery as normal, or reduced to 75% of normal	[27,28]
Porosity	0.52	0.49	Mean porosity determined from the 5 blocks for each type
Permeability	10^{-10} m^2		[18]

3. In the same geometries as described in scenarios 1 and 2 but with the addition of septal veins in addition to decidual veins. Little is published on the anatomy of these septal veins, but they have been identified in placental tissue [29]. Here they are assumed to reside at 1/3 and 2/3 of the height Z_p and to be half the diameter of decidual veins (d_V/2).
4. In the same geometries as described for a normal term placenta in scenarios 1 and 3 but without central cavities, which have been suggested to have functional importance as highways for maternal blood to penetrate deep into the IVS [30].

In some cases, the parameters above differ from those used in our 2D placentone models. In particular, spiral artery diameter and placentone height differ. In prior work spiral artery mouth diameter was informed by ultrasound data of spiral artery jets, which may overestimate mouth size due to resolution [18]. Here, we have decreased this parameter to values more similar to diameters reported in Harris and Ramsey [23] and used in 2D models in Burton et al. [24]. In the FGR scenario we arbitrarily decreased this diameter by 50% to explore the effect of impaired remodelling. Reports of placentone height (placental thickness) vary in the literature, and can be confounded by wide gestational age ranges. Here we refined our prior estimates of normal placentone height (24 mm [6]) to align this better with *in vivo* placental thicknesses as measured by ultrasound (preventing gravity induced collapse of the IVS), to fall midway in the range reported for normal placenta by Rawal et al., 2024 (25.7-38.9 mm [25]). Following data from Mathai et al., 2013, placentone height was not altered in FGR as no significant differences between normal and FGR placental thicknesses were observed when gestational age was taken into account [26].

Villous tissue model: At the scale of the villous tissue cubes, the segmented IVS was converted to an unstructured tetrahedral volume mesh using Ansys ICEM (Ansys Inc., 2022 R2). Blood flow in the IVS was explicitly simulated using the Navier Stokes equations using Ansys Fluent (Ansys Inc., 2022 R2) using fixed pressure boundary conditions on inlet and outlet faces of the tissue cubes, and symmetry conditions on the remaining faces. Convergence assessments are described in detail by Lee et al. [6]. The model output of interest is, for a given pressure drop across the imaged tissue cube, the distribution of shear stress within that cube.

Combined model: Lee et al. demonstrated that IVS flow is in the Stoke's flow regime, and so the villous tissue model results may be scaled to represent the distribution of shear stress based on pressure gradients predicted by the porous medium model of the placentome, i.e. the distribution of pressure drop illustrated in Fig. 1D and E. This allows generation of the distribution of shear stress within the placentome that accounts for regional variation in maternal flow (for example near and far from the spiral arteries). This combined model is used to predict cumulative distributions of shear stress experienced by villous tissue, with the 95th centile used as a benchmark (i.e. the value of shear stress that 95% of villous tissue experiences less than).

2.5. Immunohistochemistry

Tissue biopsies were taken from FGR (n = 10) and gestational age-matched normal third trimester placentae (n = 9), snap-frozen, cut into 5 μm sections, and fixed with acetone. To determine syncytiotrophoblast expression of mechanosensing proteins, sections were blocked with 100 μL of 10% Normal Goat Serum (NGS) in PBS-Tween (PBS-T) for 1 h at room temperature (RT), then incubated with 100 μL of the primary antibody (1.25 μg/mL anti-Dynein-1 (ab23905, Abcam, UK), 8 μg/mL Kinesin (ab15486, Abcam, UK), 5 μg/mL IFT88 (PA5-44087, Thermofisher, USA), 10 μg/mL Polycystin-2 (BS-2158R, Thermofisher), 3 μg/mL TRVP6 (PA5-51295, Thermofisher)), or 1 μg/mL Piezo-1 (602752, Biolegend, USA) diluted in 10% NGS in PBST for 1 h at RT. Literature searches were used to determine that all primary antibodies were specific for the desired epitope. After washing thrice with PBST, 100 μL of 4 μg/mL biotinylated goat anti-mouse (JI115065072, Jackson ImmunoResearch, USA), goat anti-rabbit secondary antibody (JI111065046, Jackson ImmunoResearch) or goat anti-rat secondary antibody (JI112066062, Jackson ImmunoResearch) in 10% NGS in PBST was added for 1 h at RT. Slides were washed thrice with PBST, then 100 μL of 2.5 μg/mL Streptavidin-594 in 10% NGS in PBST was added for 1 h at RT. After a final PBST wash step, 100 μL of 0.5 μg/mL Hoechst 33342 (Sigma-Aldrich, Israel) in PBST was added to slides for 5 min at RT. Sections were washed with PBST and coverslips were mounted with Citifluor (Electron Microscopy Services, USA). Irrelevant IgG1 (02-6100, Thermofisher) or IgG2 (cat no. ab172730, Abcam) antibodies at the same concentration as primary antibodies were used as negative controls (IgG1 for Kinesin and Piezo-1, IgG2 for Dynein, IFT88, Polycystin-2, TRVP6). Sections were imaged using an Olympus Slideview VS200 slide scanner with a X-Cite Xylis LED Fluorescence Light Source (XT720S) running Olympus Slideview VS200 ASW software (v4.1).

Quantitative analysis of staining intensity in the syncytiotrophoblast was performed on five regions of interest (ROI) per slide using FIJI [31]. To mitigate the autofluorescence of placental tissue, thresholding was utilised to remove autofluorescence based on the negative staining controls prior to mean pixel intensity for the Strep-594 channel being calculated using the "Measure" function. As fetal endothelial cells within the villous core also stain for mechanosensitive ion channels, to specifically quantify syncytiotrophoblast expression the villous core was removed from analysis using combined thresholding and rendering, prior to analysis. Mean pixel intensity (MPI) measurements between FGR and normal placentae were compared using unpaired non-parametric Mann-Whitney t-tests in GraphPad Prism 10 (GraphPad Software, USA). P-values <0.05 were considered statistically significant.

3. Results

3.1. The effect of FGR on flow in the IVS and syncytiotrophoblast shear stress

First, we sought to establish placentone scale porous media models

(parameterised to normal term and FGR scenarios, as in Table 1) to determine the expected velocities in the IVS and hence the pressure gradients that drive flow around the villous tissue. These models predict that the FGR placentone has a larger region of high velocity flow (>0.5 mm/s) near the spiral artery mouth (Fig. 2A and B). Notably, in this work, placental tissue samples from normal and FGR placentae used to inform models did not have significantly different average porosities (FGR 0.49 ± 0.04 SEM, normal 0.52 ± 0.07 SEM, p = 0.70), and thus this increase in the proportion of tissue exposed to higher velocity flow is primarily driven by the smaller diameter of the spiral artery mouth in the FGR model.

These porous media models allow us to determine variation in shear stress at the placentone level due to the differences in velocity distribution around the placentone, but do not allow us to determine variation in shear stress due to the microstructure of the placental tissue. Hence, to explicitly calculate shear stress within the microstructure of the placental tissue, we established tissue-level computational fluid dynamics models using blocks of villous tissue segmented from microCT imaging. These models were used to predict shear stress for a defined pressure gradient of 1 kPa/m (Fig. 2C). These results can be scaled proportionally (linearly) to predict the shear stress for higher pressure gradients up to a pressure gradient of at least 400 kPa/m [6]. The villous anatomy in FGR tissue blocks consistently resulted in predictions of higher syncytiotrophoblast shear stress, based on explicit simulations (Fig. 2C), although greater variability in the range of predicted shear stresses was observed in FGR. At 1 kPa/m driving pressure the median shear stress predicted within a tissue block is 1.6 times higher in FGR compared to normal placentae (0.059 dyn/cm^2 for FGR placenta, 0.037 dyn/cm^2 for normal placenta), and the 95th centile shear stress predicted with a block is 1.4 times higher in FGR (0.50 dyn/cm^2 for FGR, 0.36 dyn/cm^2 for normal).

Having established both placentone and tissue level models, we then combined them to make an overall prediction of syncytiotrophoblast shear stress across the placentone that accounts for both a) the variation in shear stress arising from different pressure gradients in the placentone and b) the variation in shear stress from the tissue level model. To provide an estimate for shear stress distribution across the placentone, we scale the median shear stress predicted from our tissue level model by the local pressure gradient simulated by the placentone model, allowing visualisation of shear stress levels in the placentone (Fig. 3A and B). We note that there is local micro-scale variation from this median that is not visualised. Both normal and FGR placentone models predict a 'region of influence' of the high shear stress (>0.1 dyne/cm^2 (0.01Pa)) near the spiral artery openings, after which predicted shear stress rapidly declines in more distal tissue regions. In the FGR model, this region of influence impacts a greater proportion of the tissue, and overall more villous tissue is exposed to higher levels of shear stress (indicated by deeper location within the placenta of shear stress isobars shown in Fig. 3A and B). This is reflected in a shift to the right in the cumulative distribution of shear stress in FGR compared to normal placentones (Fig. 3C). Finally, peak shear stresses are predicted to be higher in FGR with the 95th centile for shear stress 2.6 dyn/cm^2 (0.26 Pa) in the FGR model, compared to 1.2 dyn/cm^2 (0.12 Pa) in the normal model. These differences in peak shear stresses between normal and FGR placentones are particularly evident in regions at the end of the central cavity (Fig. 3A and B), and it is feasible that this could result in localised pathological impacts to tissue function in these regions. Predictions of shear stress at other percentiles can be found in Supplementary Table 3.

The above models were conducted with the same flow boundary conditions at the spiral artery inlet, but with impaired spiral artery remodelling (ie reduced diameter of the funnel region). Changes in spiral artery geometry impact velocity of flow into the IVS [24], but in addition to this impaired remodelling of the upstream uterine vessels (uterine, arcuate and radial arteries) has significant impacts on overall volumetric delivery of blood to the IVS [32–34]. To account for this, we thus also consider the case where volumetric flow rate to the placenta is reduced in FGR. Compared to FGR geometries as presented above, reducing inlet flow to the spiral arteries by 25% reduced the 95th centile shear stress from 2.6 dyn/cm^2 (0.26 Pa) to 1.7 dyn/cm^2 (0.17 Pa), but it remains elevated compared to the normal case 95th centile shear stress of 1.2 dyn/cm^2 (0.12 Pa) (Supplementary Fig. 2).

3.2. The influence of location of venous drainage on model predictions

Decidual veins have been described in the literature [23,35–38], but their dimensions and proximity to spiral arteries have not been well quantified. Classically the placentone has been modelled with a single spiral artery and two draining veins [4,6,17,18,30]. However, the location of draining veins can influence local haemodynamics [19,20], and veins that drain the IVS from the septa that sit between placentones [29] have not been previously considered in models predicting shear stress on the syncytiotrophoblast. Here, we consider the effect septal veins may have on predicted shear stress in the combined model, as this provides a significant anatomical perturbation. To explore the functional impact of septal veins, we consider 3 possible scenarios; 1) the

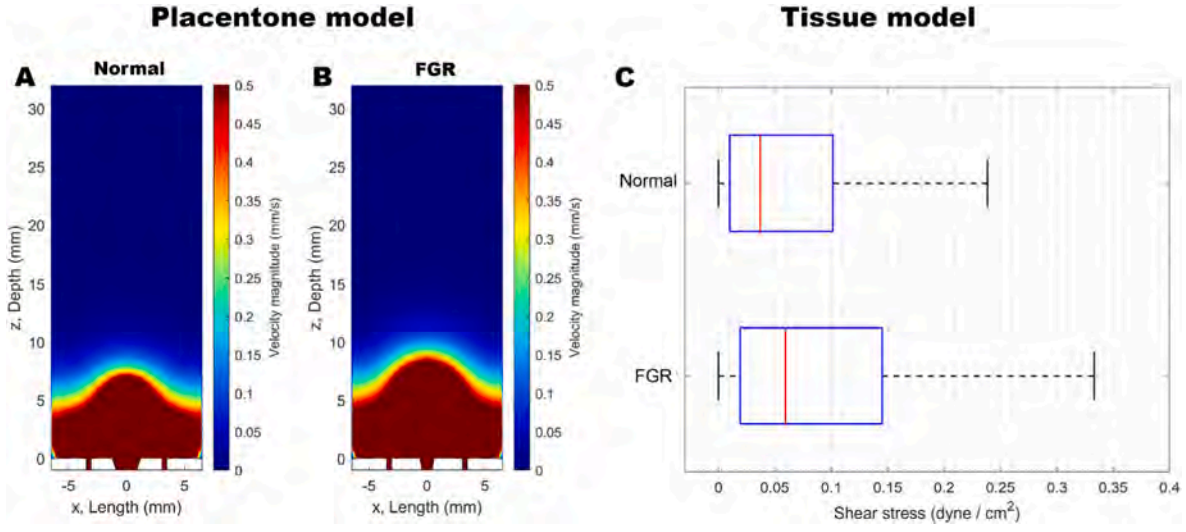

Fig. 2. Velocity maps obtained from simulations of the placentone model in A) normal and B) FGR placentones. C) The distribution of shear stress in blocks of tissue at term in normal and FGR placentae (combined predictions from n = 5 tissue blocks of each type).

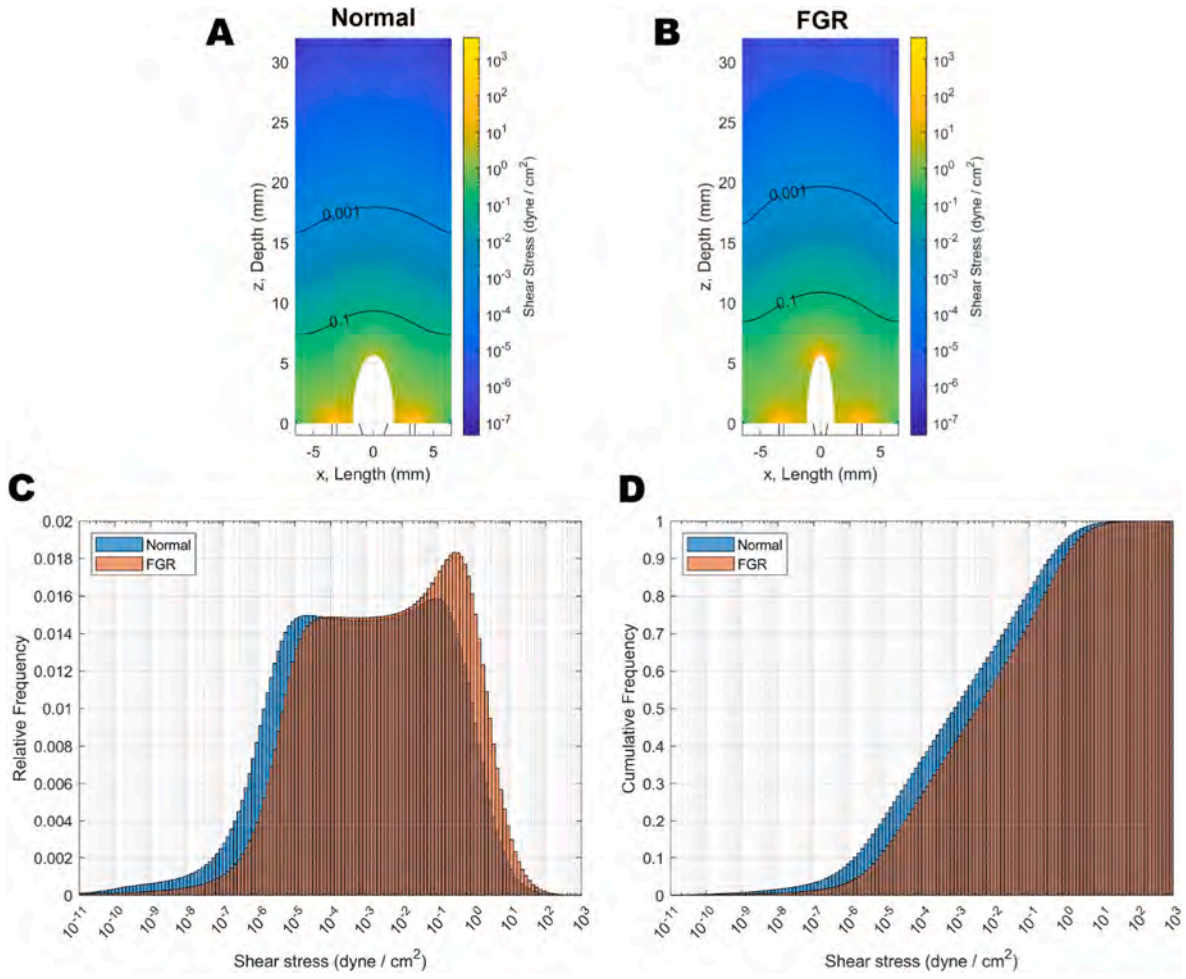

Fig. 3. The distribution of median shear stress for (A) normal placentae and (B) FGR placentae. (C) relative frequency and (D) cumulative distribution of shear stress in the whole placentone comparing normal and FGR placentae.

case where we have two septal veins on opposite sides of the placenta, both located one third of the way into the placentone ($Z_p/3$) (Fig. 4A–E), 2) the case where we have two septal veins located two thirds of the way into the placentone ($2Z_p/3$) (Fig. 4B–F), and 3) the case where we have four septal veins located at both $Z_p/3$ and $2Z_p/3$ (Fig. 4C–G). Model predictions show that the inclusion of septal veins increases penetration of blood into the IVS, especially when they are located deeper into the tissue ($2Z_p/3$, Fig. 4B and C). In all cases, there is an increase both in median shear stress throughout the IVS, and in the proportion of tissue exposed to higher levels of shear stress, compared to when septal veins are absent, with additional higher velocity 'regions of influence' of both the spiral arteries and the draining veins. Whilst simulations presented here focus on modelling the impact of septal veins in normal geometries, their influence is qualitatively similar in both normal and FGR models (Supplementary Fig. 3).

3.3. Influence of central cavity on model predictions

We have previously demonstrated in 2D models [30] and 3D porous media models [18] that central cavities (regions of sparser tissue proximal to spiral artery openings) have functional importance in ensuring perfusion of maternal blood deep into the IVS. Thus finally we used our combined model to explore the interplay between the functional impact of these central cavities and that of septal veins demonstrated above, we repeated the simulation with four septal veins above (Fig. 4C–G) but without a central cavity (Fig. 4D–H) and for completeness, the case with no central cavity and no septal veins (Supplementary Fig. 4B and F). This demonstrates that the septal veins and central cavity have a synergistic impact on penetration of blood into the placenta, with increased flow velocity through the IVS, and a greater region of tissue exposed to shear stresses >0.1 dyne/cm^2 (0.01Pa) when both are present. We also confirm the importance of the central cavity itself on perfusion of blood into the IVS using this model, with very low flow velocities present in the absence of a central cavity or septal veins (Supplementary Fig. 4B and F). Indeed, changes in the shape of the velocity profile when a central cavity is present (with or without septal veins) highlight that these cavities are required for the presence of focused high velocity jets that have been observed in ultrasound [18,27].

3.4. Syncytiotrophoblast expression of the mechanosensing proteins Dyenin-1, Kinesin-2 and TRVP6 is altered in FGR

The ability of the placenta to respond to changes in shear stress predicted in FGR above is dependent on the expression of mechanosensing proteins on the syncytiotrophoblast. However, it is also possible that mechanosensor expression changes in FGR, either independently of, or in response to, changes in syncytiotrophoblast shear stress. To examine this we undertook immunohistochemical analysis of mechanosensitive motor proteins (Dyenin-1, Kinesin-2, IFT88) and ion channels (Polycystin-2, TRVP6, Piezo-1) [6] in placental biopsies from normal (n = 9) and FGR (n = 10) placentae. In all tissues, microtubular motor protein expression was restricted to the syncytiotrophoblast, whereas expression of mechanosensitive ion channels was observed in both the syncytiotrophoblast and endothelial cells within the placenta

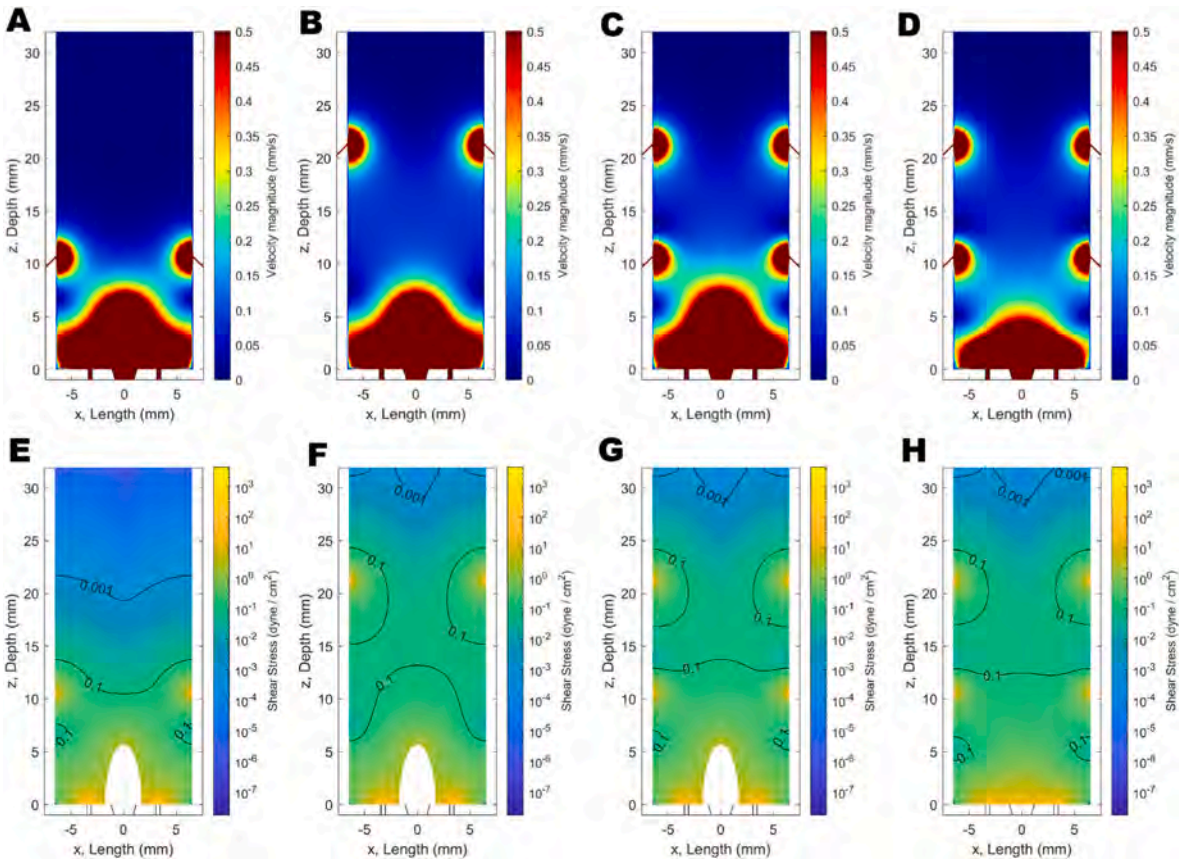

Fig. 4. The impact of septal vein location on velocity (A, B, C, D) and predicted median shear stress (E, F, G, H) in the normal placentone model. Septal veins were modelled in opposing pairs at one third depth (A, E) or two thirds depth (B, F) or as four veins at both one third and two thirds depth (C, G). While (D, H) shows the case of four veins at both one third and two thirds depth but with no central cavity present. All images depict a plane passing through the centre of the placentone that intersects with the decidual veins. Contour lines represent 0.1 or 0.001 dyne/cm^2 of shear stress.

(Fig. 5). No changes in the staining intensity of mechanosensing proteins were observed across the depth of the placental tissue (chorionic, middle, near-maternal, Supplementary Fig. 14). Quantitative comparisons of staining intensity (MPI) demonstrated that Dyenin-1 had a significantly greater intensity in the syncytiotrophoblast of FGR placentae compared to normal placentae (FGR MPI = 4682 ± 91.3 SEM vs normal MPI = 4278 ± 83.6 SEM, p = 0.0350, Fig. 5A, B, D). In contrast, the syncytiotrophoblast of FGR placentae had significantly lower staining intensity of Kinesin-2 (FGR MPI = 2645 ± 48.7 SEM, vs. normal MPI = 2866 ± 80.6 SEM, p = 0.0350, Fig. 5E, F, H) and TRPV6 (FGR MPI = 1679 ± 16.6 SEM, vs. normal MPI = 1823 ± 51.6 SEM, p = 0.003, Fig. 5Q, R, T). No significant difference in the intensity of IFT88, Polycystin-2 or Piezo-1 staining was observed between normal and FGR placentae (p > 0.6, Fig. 5I, J, L,M, N, P,U, V,X).

4. Discussion

Our use of anatomically-informed multi-scale models of IVS blood flow in this work have allowed us to explore the different anatomical contributors to differences in blood flow velocity and shear stress across the depth of the placenta in normal and FGR scenarios. These predictions highlight the impact of impaired spiral artery remodelling in increasing blood flow velocity (and thus syncytiotrophoblast shear stress) near the spiral artery mouth as considered previously [24,39] but extend this notion to demonstrate that an interplay between spiral artery flows and the villous tissue architecture contribute to the increased syncytiotrophoblast shear stress predicted in FGR. In addition, by exploring the impact of recently documented septal veins on IVS perfusion we demonstrated that these act synergistically with the central cavities proximal to spiral artery openings to increase the extent of IVS perfusion.

Median levels of shear stress reported in this work (0.00094 dyne/cm^2 for normal cases, 0.0039 dyne/cm^2 for FGR) are both lower than those previously reported in 2D modelling approaches of normal term placentae by ourselves (0.04 dyne/cm^2 median shear stress) [6] and others (0.5-2.3 dyne/cm^2 range of shear stress) [4]. This difference predominantly arises from the impact of the 3D space on the median value as the proportion of villous tissue further away from the inlet and outlet is greater in 3D than in 2D. Roth et al. also adopted a 3D approach but their model considers a smaller region of ~2 mm of tissue near the spiral artery mouth, and thus is not impacted by 3D volume to the same extent as our model of the entire placentone [5]. Median shear stress could not be extracted from Roth et al., however, their visualisations suggest peak shear stress <40 dyne/cm^2 (4 Pa), with most tissue near the spiral artery mouth <10 dyne/cm^2 (1 Pa) [5]. We do see peak shear stresses of similar magnitude in our models (see Supplementary Material), but this is similarly limited to small regions near the spiral artery mouth, with our model suggesting a 95th centile shear stress of 1.2 dyn/cm^2 (0.12 Pa). All simulation studies show a wide range of shear stress over the areas or volumes considered, due to a transition from high velocity flow near the spiral arteries and a much slower flow of blood around more distal villi. Therefore, median values of shear stress may not be reflective of the range of physiology expected.

The flow patterns observed in our models are similar to those found in a 3D-printed human cotyledon model imaged by MRI [39] and in 3D computational fluid dynamics simulations [20] with high velocities primarily concentrated at the central cavity. Similar to these other approaches, we observe that impaired spiral artery remodelling in FGR has

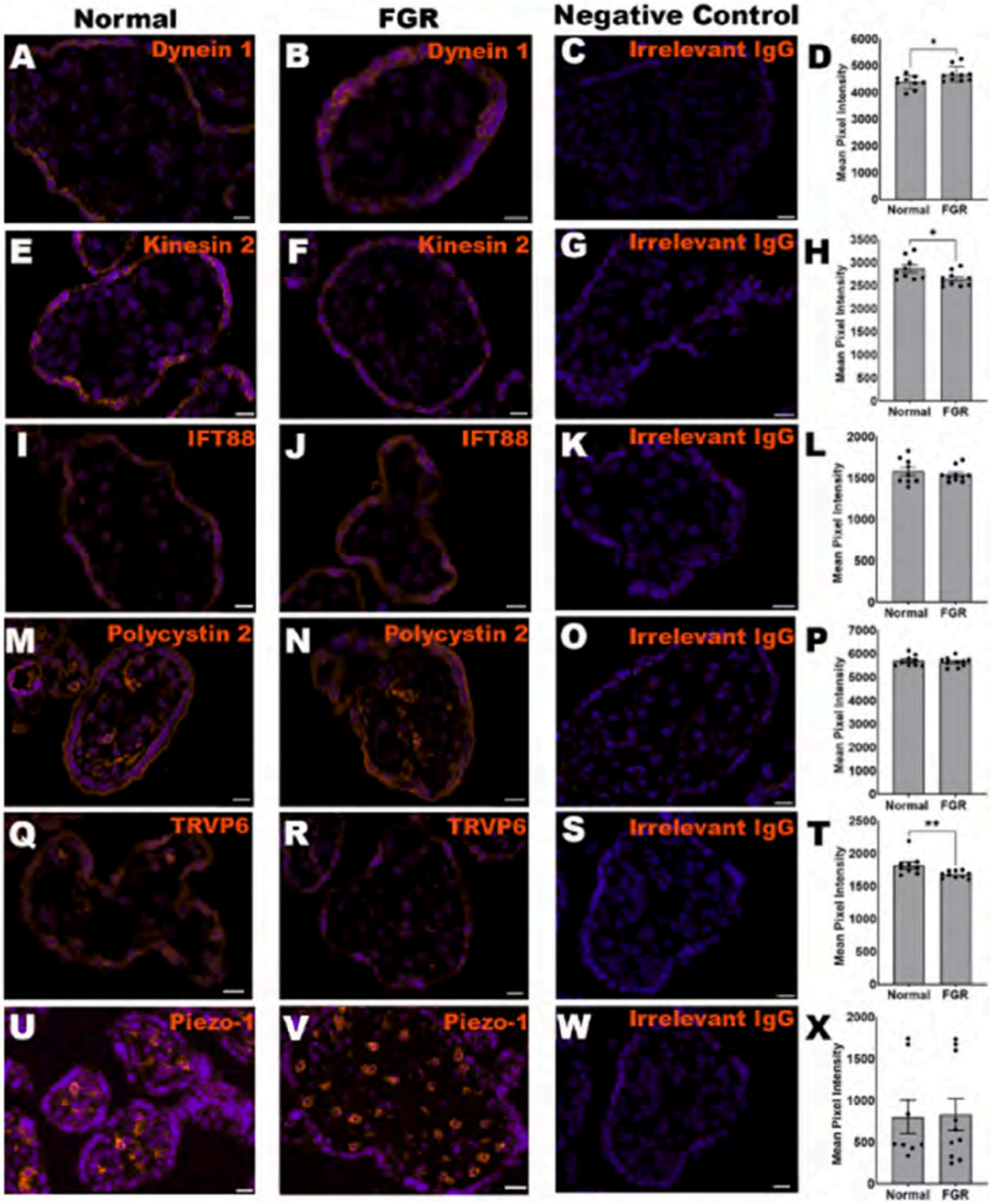

Fig. 5. Mechanosensing protein expression in normal and FGR placentae**.** Representative images showing immunofluorescent staining of normal (A,E,I,M,Q,U) or FGR (B,F,J,N,R,V) placental tissue with antibodies reactive with Dyenin-1 (A, B), Kinesin-2 (E, F), IFT88 (I, J), Polycystin-2 (M, N), TRVP6 (Q, R) or Piezo1(U, V). Third trimester tissue stained with irrelevant IgG (C,G,K,O,S,W) antibodies were used as negative controls. Nuclei are counterstained with Hoechst-3342 (blue). Scale bars = 20 μm. Bar graphs show the Mean Pixel Intensity of Dynein 1 (D), Kinesin 2 (H), IFT88 (L), Polycystin 2 (P), and TRVP6 (T) and Piezo-1 (X) on the syncytiotrophoblast only from normal (n = 9) or FGR (n = 10) placentae. Error bars = SEM, *p-value <0.05, ** p-value <0.01. (For interpretation of the references to colour in this figure legend, the reader is referred to the Web version of this article.)

a strong impact on the velocity of blood entering the placentone, in turn resulting in and deeper penetration of high velocity flow into the IVS. In addition to these changes seen at the placentone level, our approach allows us to quantify the effect of changes in villous tissue architecture in FGR for the first time. This highlights the additional impact that even relatively small anatomical differences in tissue architecture and villous density in FGR can have on syncytiotrophoblast shear stress, which combine with uterine changes at the placentone level to produce higher velocity flows in the IVS in FGR.

In light of the above, our data critically highlights the importance of thinking beyond mean/median levels of 'high' and 'low' shear stress to more physiologically consider how the range of shear stresses change dynamically across the IVS, and how this may impact local tissue function. In both normal and FGR scenarios our models predict that

large regions of the syncytiotrophoblast are exposed to relatively low levels of shear stress (<0.1 dyne/cm^2). Such shear stress conditions (0.001-0.1 dyne/cm^2) have previously been demonstrated to enhance syncytiotrophoblast formation and hCG production relative to static cultures [40,41], indicating that these conditions allow for physiologically normal tissue function. However, in FGR a greater proportion of tissue is predicted to be expose to shear stresses 0.1 dyne/cm^2 or higher. This may have functional impacts, as 0.1 dyne/cm^2 flow has been reported to reduce the length of microvilli on the syncytiotrophoblast relative to regions of 0.001 dyne/cm^2 flow [13], and thus greater proportions of tissue impacted by shear stress at this level (as we predict in FGR) could reduce the overall surface area for exchange in a manner that extends beyond reduced villus branching/tissue density. Exchange may also be impacted by changes in local IVS blood flow velocities, due to local maternal-fetal flow matching. This was not explicitly modelled in this study, unlike in prior porous media approaches [17,30], but coupling to oxygen transport and exchange models may be a future extension to this modelling approach both at the tissue and placentone scale.

One of the most notable physiological differences in shear stress conditions within the IVS in our models arose at regions proximal to spiral artery mouths and sites of venous drainage, where a much greater proportion of tissue is regionally exposed to peak levels of shear stress. High levels of shear stress are thought to impair syncytiotrophoblast function, potentially leading to increased shedding of pro-inflammatory material, or deposition of fibrin that can reduce exchange capacity [12,24]. However, it is notable that *in vitro* studies to date have not explicitly considered the impacts of high but physiologically-relevant levels of syncytiotrophoblast shear stress predicted in our models (0.1-2.6 dyne/cm^2), with most studies designed around median values (0.001-0.1 dyne/cm^2 [13,40,41]), or conducted in more complex/-longer term 3D tissue flow systems in which explicit levels of shear stress on the syncytiotrophoblast are more complex to define [12,42]. Those studies that have considered impacts of flows of 1 [43] or 10 dyne/cm^2 [11] (which broadly show improved syncytiotrophoblast differentiation and hormone production relative to static conditions) have not considered how parameters change under different levels of shear stress, or examine functional aspects of the syncytiotrophoblast that may relate to the pathophysiology of FGR such as syncytiotrophoblast thickness, fibrin deposition, or shedding. Thus, there is clear need for future studies to better understand how the key difference in peak levels of shear stress regionally predicted proximal to the spiral artery mouths in FGR impacts syncytiotrophoblast function and villous development, in particular with respect to the evolution of central cavities of less dense villous tissue in these regions of peak shear stress throughout gestation [18].

We explored the effect of regional heterogeneity in flows via explicit consideration of the impact of central cavities and septal veins on blood flow velocity and syncytiotrophoblast shear stress in our model. Consistent with our prior work simulating the impact of central cavities [6,30], the model illustrated that inclusion of these structures improved perfusion of blood through the IVS, and increased the proportion of tissue exposed to higher velocity and shear. Secondly, we considered the impact of septal veins, with models predicting that these structures increase blood flow and perfusion in the IVS, with scenarios that included veins that were more distal to the spiral arteries having the largest impact. Inclusion of central cavities and veins in the models resulted in higher levels of velocity throughout the IVS (indicative of greater perfusion). It is notable that inclusion of central cavities and septal veins had similar impacts on velocity and shear stress in both normal and FGR scenarios, highlighting the extent of functional impact of these structures, and the importance of quantifying how they change in pathology in future work.

The syncytiotrophoblast of FGR placentae exhibited altered mechanosensing protein expression, with higher expression of Dynein-1, but lower expression of Kinesin-2 and TRPV6. Mechanosensing proteins detect shear stress and initiate signaling cascades that are integral to tissue morphogenesis [44]. As Dyein-1 and Kinesin-2 are both mechanosensitive motor proteins, their differential direction of regulation was initially surprising, but may result from their differential functions. Dyenin-1 triggers retrograde transport of intracellular components along microtubules, potentially initiating autophagy to remove damaged cellular components, and thus increased expression in FGR may be indicative of heightened damage repair mechanisms [45]. Kinesin-2, an essential anterograde motor protein, is responsible for establishing cell polarity and playing roles in cilia formation in other tissues [46,47] and thus reduced Kinesin-2 expression is in line with reduced microvillus density and function in FGR. Finally, our work showed decreased levels of the mechanosensitive ion channel TRPV6 on the syncytiotrophoblast of FGR placentae. Shear stress-induced opening of TRVP6 facilitates a Ca^{2+} influx into cells that can activate intracellular signaling cascades critical for syncytiotrophoblast microvilli formation [13]. Knockdown of TRVP6 decreased the density of syncytiotrophoblast microvilli on syncytialised BeWo cells [13] and in murine models [48]. Thus reduced TRVP6 expression in FGR may similarly reduce syncytiotrophoblast microvilli formation reducing the surface area for exchange and impairing biomechanical signaling via reduced Ca^{2+} influx.

Whilst our modelling data demonstrates that greater regions of tissue are exposed to higher shear stress in FGR, the greatest variation in shear stress occurs across the depth of the tissue (with villi more distal to spiral artery openings (or veins) experiencing much lower shear stresses). Thus, the fact that mechanosensing protein expression does not vary across different depths of tissue (ie near-maternal to chorionic, Supplementary Fig. 14) suggests that the differences we see in mechanosensing protein expression in FGR are not a result of differences in tissue exposure to shear stress, but rather are intrinsic to the tissue itself. This highlights that both a) the levels of syncytiotrophoblast shear stress and b) the ability of the tissue to respond to that shear stress, may act synergistically to impact syncytiotrophoblast function in FGR. Finally, as our previous work has shown elevated levels of mechanosensing protein expression in the syncytiotrophoblast in early gestation [6], it is interesting to consider how the interactions between syncytiotrophoblast shear stress and mechanosensing protein expression play out in the pathophysiological origins of FGR in early pregnancy. Future work employing cell culture models will be important to better elucidate the mechanisms by which the interplay between shear stress, mechanosensation, and the resulting downstream signaling cascades may impact trophoblast function and placental development from early in gestation.

4.1. Limitations

One of the primary limitations of our current approach is the assumption that the placentone has a homogeneous spatial porosity and permeability. Our microCT data suggests no significant difference in villous tissue density with depth of the placenta (Supplementary Material). However, it is likely that, for example, localisation of stem villi would lead to locally different porosity to a region with predominantly terminal villi. Analysis of imaging and explicit simulation of flow around the villous structure in 3D is prohibitively computationally expensive. In our placentone model we effectively smooth the true anatomical variation, which our microCT data suggests is reasonable at scales of ~1.5 mm^3, however, a formal analysis of the scales at which homogenisation is reasonable was not conducted [49]. Samples used for microCT imaging in this work were not perfusion fixed, and hence it is important to acknowledge that they likely underestimate *in vivo* IVS porosity as some gravitational collapse of the placental tissue occurs when the IVS is not under pressure. As a result, our absolute predictions of shear stress may tend to over-estimate *in vivo* values. However, under the assumption that this tissue collapse impacts normal and FGR groups in the same way, useful comparisons can still be drawn between these two groups.

Limitations on our anatomical understanding also exist in uterine

parameterisation of the model. We have adopted the approach of assuming a single spiral artery and two outlet decidual veins (as is typically modelled [4,6,18,20]) but acknowledge that it may be possible for more than one spiral artery to feed a placentone in some circumstances, and that the number and size of decidual/septal veins are not well described in the literature. Uterine tissue in pregnancy is difficult to directly access, but *in vivo* imaging studies that can assess flow of blood at the decidual-placental interface and are rapidly increasing in resolution may improve our understanding of this interface in the future [50,51]. Nonetheless, our exploratory approach demonstrates the potential functional importance of the number of and location of decidual vessels, and could be refined further in the future as more data becomes available. The location of septa in relation to placentones (a functional unit with one villous tree and one spiral artery) is also idealised for modelling purposes. Indeed, there may be multiple villous trees separated by septa. This assumption is common in modelling studies with no slip (wall) conditions typically applied at the placentone edges [6,17,18,20,30]. While we do model the impact of tissue heterogeneity here, we do not explicitly model villous tree structure, reducing some of the impact of this assumption. Finally, whilst our placentone models were parameterised to normal and FGR scenarios, at the organ-scale, heterogeneity can exist across the placenta, that can impact placentone size, villous density, and spiral artery perfusion. As such, future considerations of IVS flow at an organ level may provide important insights into how this heterogeneity intersects with IVS perfusion and placental exchange.

5. Conclusion

In conclusion, our work has demonstrated that in FGR impaired remodelling of the spiral arteries and changes in villous tissue architecture combine to increase the proportion of placental tissue exposed to higher shear stress, and that septal veins and central cavities may act synergistically to ensure adequate placental perfusion. Future work is needed to more explicitly quantify the extent of anatomical change in these structures in FGR. Finally, independent of shear stress exposure, differences in the expression of mechanosensing proteins on the syncytiotrophoblast in FGR, providing a further mechanistic layer by which alterations in the haemodynamic environment in the IVS in FGR may negatively impact syncytiotrophoblast function. Together, this data helps inform understanding of the structure-function relationships that govern IVS haemodynamics in FGR, and how these intersect with syncytiotrophoblast function. This is key to both better inform experimental paradigms, and to mechanistically relate utero-placental perfusion parameters to poor pregnancy outcomes.

Generative AI statement

Generative AI was not used in any aspect of this work.

Funding details

This research was supported by a Royal Society Marsden Fund Grant (22-UOA-151) and a Health Research Council of New Zealand Consolidator Grant (20/926). IR was supported by a University of Auckland Summer Scholarship. None of these funding bodies had any role in the design of this research or interpretation of the data.

CRediT authorship contribution statement

Tet Chuan Lee: Data curation, Funding acquisition, Methodology, Writing – original draft. **Teena K.J.B. Gamage:** Data curation, Investigation, Supervision, Writing – original draft. **Mary Spring:** Data curation, Writing – original draft. **Isha Ramanlal:** Formal analysis, Investigation. **Toby Jackson:** Methodology. **Alys R. Clark:** Conceptualization, Data curation, Formal analysis, Funding acquisition, Methodology, Resources, Writing – review & editing. **Joanna L. James:** Conceptualization, Data curation, Funding acquisition, Investigation, Methodology, Project administration, Resources, Writing – original draft, Writing – review & editing.

Declaration of competing interest

The authors have no competing conflicts of interest to declare.

Acknowledgments

Thanks are extended to the research midwifery team in assisting the collection of samples used in this work, as well as staff and patients at the Birthing Unit of Auckland City Hospital for donating the placental tissue.

Appendix A. Supplementary data

Supplementary data to this article can be found online at https://doi.org/10.1016/j.placenta.2026.07.007.

References

[1] S.J. Gordijn, I.M. Beune, B. Thilaganathan, A. Papageorghiou, A.A. Baschat, P. N. Baker, R.M. Silver, K. Wynia, W. Ganzevoort, Consensus definition of fetal growth restriction: a Delphi procedure, Ultrasound Obstet. Gynecol. 48 (3) (2016) 333–339.
[2] F. Figueras, J. Gardosi, Intrauterine growth restriction: new concepts in antenatal surveillance, diagnosis, and management, Am. J. Obstet. Gynecol. 204 (4) (2011) 288–300.
[3] C. Sun, K.M. Groom, C. Oyston, L.W. Chamley, A.R. Clark, J.L. James, The placenta in fetal growth restriction: what is going wrong? Placenta 96 (2020) 10–18.
[4] E. Lecarpentier, M. Bhatt, G.I. Bertin, B. Deloison, L.J. Salomon, P. Deloron, T. Fournier, A.I. Barakat, V. Tsatsaris, Computational fluid dynamic simulations of maternal circulation: wall shear stress in the human placenta and its biological implications, PLoS One 11 (1) (2016) e0147262.
[5] C.J. Roth, E. Haeussner, T. Ruebelmann, F.V. Koch, C. Schmitz, H.G. Frank, W. A. Wall, Dynamic modeling of uteroplacental blood flow in IUGR indicates vortices and elevated pressure in the intervillous space - a pilot study, Sci. Rep. 7 (2017) 40771.
[6] T.C. Lee, A. Moulvi, J.L. James, A.R. Clark, Multi-scale modelling of shear stress on the syncytiotrophoblast: could maternal blood flow impact placental function across gestation? Ann. Biomed. Eng. 51 (6) (2023) 1256–1269.
[7] T. Mayhew, J. Wijesekara, P. Baker, S. Ong, Morphometric evidence that villous development and fetoplacental angiogenesis are compromisd by intrauterine growth restriction but not by pre-eclampsia, Placenta 25 (2004) 829–833.
[8] J. Kingdom, B. Huppertz, G. Seaward, P. Kaufmann, Development of the placental villous tree and its consequences for fetal growth, Eur. J. Obstet. Gynecol. Reprod. Biol. 92 (1) (2000) 35–43.
[9] P. Patwari, R.T. Lee, Mechanical control of tissue morphogenesis, Circ. Res. 103 (3) (2008) 234–243.
[10] B. Fels, K. Kusche-Vihrog, It takes more than two to tango: mechanosignaling of the endothelial surface, Pflugers Arch 472 (4) (2020) 419–433.
[11] A. Inohaya, Y. Chigusa, M. Takakura, S. Io, M.A. Kim, Y. Matsuzaka, E. Yasuda, Y. Ueda, Y. Kawamura, S. Takamatsu, H. Mogami, Y. Takashima, M. Mandai, E. Kondoh, Shear stress in the intervillous space promotes syncytial formation of iPS cells-derived trophoblastsdagger, Biol. Reprod. 110 (2) (2024) 300–309.
[12] B.A. Brugger, L. Neuper, J. Guettler, D. Forstner, S. Wernitznig, D. Kummer, F. Lyssy, J. Feichtinger, J. Krappinger, A. El-Heliebi, L. Bonstingl, G. Moser, G. Rodriguez-Blanco, O.A. Bachkonig, B. Gottschalk, M. Gruber, O. Nonn, F. Herse, S. Verlohren, H.G. Frank, N. Barapatre, C. Kampfer, H. Fluhr, G. Desoye, M. Gauster, Fluid shear stress induces a shift from glycolytic to amino acid pathway in human trophoblasts, Cell Biosci. 13 (1) (2023) 163.
[13] S. Miura, K. Sato, M. Kato-Negishi, T. Teshima, S. Takeuchi, Fluid shear triggers microvilli formation via mechanosensitive activation of TRPV6, Nat. Commun. 6 (2015) 8871.
[14] N. Montalbetti, Q. Li, Y. Wu, X.Z. Chen, H.F. Cantiello, Polycystin-2 cation channel function in the human syncytiotrophoblast is regulated by microtubular structures, J. Physiol. 579 (Pt 3) (2007) 717–728.
[15] L. McCowan, K. Groom, A. Stewart, The use of customised versus population-based birthweight standards in predicting perinatal mortality, BJOG 114 (10) (2007) 1302–1303, author reply 1303.
[16] P.A. Yushkevich, J. Piven, H.C. Hazlett, R.G. Smith, S. Ho, J.C. Gee, G. Gerig, User-guided 3D active contour segmentation of anatomical structures: significantly improved efficiency and reliability, Neuroimage 31 (3) (2006) 1116–1128.
[17] I.L. Chernyavsky, O.E. Jensen, L. Leach, A mathematical model of intervillous blood flow in the human placentone, Placenta 31 (1) (2010) 44–52.

[18] R. Saghian, J.L. James, M.H. Tawhai, S.L. Collins, A.R. Clark, Association of placental jets and mega-jets with reduced villous density, J. Biomech. Eng. 139 (5) (2017).
[19] T. Mekler, R. Plitman Mayo, J. Weissmann, G. Marom, Impact of tissue porosity and asymmetry on the oxygen uptake of the human placenta: a numerical study, Placenta 129 (2022) 15–22.
[20] A. Najmi, N.G. Gutiérrez, Computational modeling of a human placentone: simulating uteroplacental hemodynamics, Phys. Fluids 36 (12) (2024).
[21] A.R. Pries, T.W. Secomb, P. Gaehtgens, Biophysical aspects of blood flow in the microvasculature, Cardiovasc. Res. 32 (4) (1996) 654–667.
[22] I. Brosens, W. Robertson, H. Dixon, The role of the spiral arteries in the pathogenesis of pre-eclampsia, Obstet. Gynecol. Annu. 1 (1972) 177–191.
[23] J. Harris, E. Ramsey, The morphology of human uteroplacental vasculature, Contribut. Embryol. 38 (1966) 43–53.
[24] G. Burton, A. Woods, E. Jauniaux, J. Kingdom, Rheological and physiological consequences of conversion of the maternal spiral arteris for uteroplacental blood flow during human pregnancy, Placenta 30 (2009) 473–482.
[25] S. Rawal, S. Ray, N. Sharma, Correlation between ultrasonographic placental thickness and adverse fetal and neonatal outcomes, Cureus 16 (3) (2024) e56410.
[26] B.M. Mathai, S.C. Singla, P.P. Nittala, R.J. Chakravarti, J.N. Toppo, Placental thickness: its correlation with ultrasonographic gestational age in normal and intrauterine growth-retarded pregnancies in the late second and third trimester, J. Obstet. Gynaecol. India 63 (4) (2013) 230–233.
[27] S.L. Collins, J.S. Birks, G.N. Stevenson, A.T. Papageorghiou, J.A. Noble, L. Impey, Measurement of spiral artery jets: general principles and differences observed in small-for-gestational-age pregnancies, Ultrasound Obstet. Gynecol. 40 (2) (2012) 171–178.
[28] S.L. Collins, G.N. Stevenson, J.A. Noble, L. Impey, Developmental changes in spiral artery blood flow in the human placenta observed with colour Doppler ultrasonography, Placenta 33 (10) (2012) 782–787.
[29] D. Amanitis, F. Deligianni, R. Abuhaimed, L. Leach, An ex-vivo macroscopic analysis of the human placental inter-lobular and inter-cotyledon septum and vessels therein from normal pregnancies, Int. Feder. Placenta Assoc. Placenta (2023) e68–e69.
[30] M. Lin, B. Mauroy, J.L. James, M.H. Tawhai, A.R. Clark, A multiscale model of placental oxygen exchange: the effect of villous tree structure on exchange efficiency, J. Theor. Biol. 408 (2016) 1–12.
[31] J. Schindelin, I. Arganda-Carreras, E. Frise, V. Kaynig, M. Longair, T. Pietzsch, S. Preibisch, C. Rueden, S. Saalfeld, B. Schmid, J.Y. Tinevez, D.J. White, V. Hartenstein, K. Eliceiri, P. Tomancak, A. Cardona, Fiji: an open-source platform for biological-image analysis, Nat. Methods 9 (7) (2012) 676–682.
[32] J.L. James, R. Saghian, R. Perwick, A.R. Clark, Trophoblast plugs: impact on utero-placental haemodynamics and spiral artery remodelling, Hum. Reprod. 33 (8) (2018) 1430–1441.
[33] A.R. Clark, J.L. James, G.N. Stevenson, S.L. Collins, Understanding abnormal uterine artery Doppler waveforms: a novel computational model to explore potential causes within the utero-placental vasculature, Placenta 66 (2018) 74–81.
[34] H.H. Allerkamp, A.R. Clark, T.C. Lee, T.K. Morgan, G.J. Burton, J.L. James, Something old, something new: digital quantification of uterine vascular remodelling and trophoblast plugging in historical collections provides new insight into adaptation of the utero-placental circulation, Hum. Reprod. 36 (3) (2021) 571–586.
[35] N. He, L. van Iperen, D. de Jong, K. Szuhai, F.M. Helmerhorst, L.A. van der Westerlaken, S.M. Chuva de Sousa Lopes, Human extravillous trophoblasts penetrate decidual veins and lymphatics before remodeling spiral arteries during early pregnancy, PLoS One 12 (1) (2017) e0169849.
[36] G. Moser, K. Windsperger, J. Pollheimer, S.C. de Sousa Lopes, B. Huppertz, Human trophoblast invasion: new and unexpected routes and functions, Histochem. Cell Biol. 150 (4) (2018) 361–370.
[37] C.M. Craven, L. Zhao, K. Ward, Lateral placental growth occurs by trophoblast cell invasion of decidual veins, Placenta 21 (2–3) (2000) 160–169.
[38] J. Boyd, W. Hamilton, The Human Placenta, W. Heffer & Sons Ltd, Cambridge, 1970.
[39] N. Barapatre, D. Frank, F.E. von Koch, S. Grundmann, H.G. Frank, M. Bruschewski, High-resolution MRI reveals uteroplacental flow dynamics in a 3D-printed human placental cotyledon model, Sci. Adv. 11 (34) (2025) eadw9753.
[40] A. Abostait, J. Tyrrell, M. Abdelkarim, S. Shojaei, W.H. Tse, I.M. El-Sherbiny, R. Keijzer, H.I. Labouta, Placental nanoparticle Uptake-On-a-Chip: the impact of trophoblast syncytialization and shear stress, Mol. Pharm. 19 (11) (2022) 3757–3769.
[41] L. Delon, M. Busek, P.D. Menezes, N. Gadegaard, J. Stokowiec, A. Golovin, Y. Boichuk, T. Combriat, A. Aizenshtadt, S. Krauss, Placental syncytium-on-chip (PSoC)-Comparison of Forskolin or mechanical induced-syncytialization, Adv. Healthcare Mater. 14 (21) (2025) e2404462.
[42] N. Kupper, E. Pritz, M. Siwetz, J. Guettler, B. Huppertz, Placental villous explant culture 2.0: flow culture allows studies closer to the in vivo situation, Int. J. Mol. Sci. 22 (14) (2021).
[43] E. Lecarpentier, A. Atallah, J. Guibourdenche, M. Hebert-Schuster, S. Vieillefosse, A. Chissey, B. Haddad, G. Pidoux, D. Evain-Brion, A. Barakat, T. Fournier, V. Tsatsaris, Fluid shear stress promotes placental growth factor upregulation in human syncytiotrophoblast through the cAMP-PKA signaling pathway, Hypertension 68 (6) (2016) 1438–1446.
[44] C.P. Heisenberg, Y. Bellaiche, Forces in tissue morphogenesis and patterning, Cell 153 (5) (2013) 948–962.
[45] A. Nambiar, R. Manjithaya, Driving autophagy - the role of molecular motors, J. Cell Sci. 137 (3) (2024).
[46] S. Fan, T.W. Hurd, C.J. Liu, S.W. Straight, T. Weimbs, E.A. Hurd, S.E. Domino, B. Margolis, Polarity proteins control ciliogenesis via kinesin motor interactions, Curr. Biol. 14 (16) (2004) 1451–1461.
[47] F. Lin, T. Hiesberger, K. Cordes, A.M. Sinclair, L.S. Goldstein, S. Somlo, P. Igarashi, Kidney-specific inactivation of the KIF3A subunit of kinesin-II inhibits renal ciliogenesis and produces polycystic kidney disease, Proc. Natl. Acad. Sci. U. S. A. 100 (9) (2003) 5286–5291.
[48] M. Winter, P. Weissgerber, K. Klein, F. Lux, D. Yildiz, U. Wissenbach, S.E. Philipp, M.R. Meyer, V. Flockerzi, C. Fecher-Trost, Transient receptor potential Vanilloid 6 (TRPV6) proteins control the extracellular matrix structure of the placental labyrinth, Int. J. Mol. Sci. 21 (24) (2020).
[49] I.L. Chernyavsky, L. Leach, I.L. Dryden, O.E. Jensen, Transport in the placenta: homogenizing haemodynamics in a disordered medium, Philos. Trans. A Math. Phys. Eng. Sci. 369 (1954) (2011) 4162–4182.
[50] G.J. Hutchinson, A. Blakey, N. Jones, L. Leach, N. Dellschaft, P. Houston, M. Hubbard, R. O'Dea, P.A. Gowland, The effects of maternal flow on placental diffusion-weighted MRI and intravoxel incoherent motion parameters, Magn. Reson. Med. 93 (4) (2025) 1629–1641.
[51] G.N. Stevenson, J.A. Noble, A.W. Welsh, L. Impey, S.L. Collins, Automated visualization and quantification of spiral artery blood flow entering the first-trimester placenta, using 3-D power doppler ultrasound, Ultrasound Med. Biol. 44 (3) (2018) 522–531.